



# Convective Mach Number and Full-Scale Supersonic Jet Noise Directivity

Kent L. Gee,\*<sup>✉</sup> Tyce W. Olaveson,<sup>†</sup> and Logan T. Mathews<sup>‡</sup>  
Brigham Young University, Provo, Utah 84602

<https://doi.org/10.2514/1.J064208>

This paper examines the connection of convective Mach number definitions to maximum noise radiation angle for a T-7A-installed GE F404 jet engine. Definitions include those corresponding to Kelvin–Helmholtz (K-H) and supersonic instability (SI) Mach waves, and an empirical formulation. Under convectively supersonic conditions without an afterburner (AB), only K-H waves are present. At AB, SI Mach waves may exist, but at shallow angles outside the main radiation lobe. Evidence suggests that Mach wave radiation from faster-than-ordinary K-H waves could stem from shock-cell velocity fluctuations. The empirical convective Mach number indicates decreasing effective convective velocity from ~80 to ~60% of fully expanded velocity as engine power increases to AB. This convective velocity decreases with frequency, especially for those whose maximum source locations occur between the potential and supersonic core tips. Additionally, a new definition of supersonic-jet convective Mach number, dependent solely on the jet acoustic Mach number,  $\sim\sqrt{M_{ac}}$ , has been derived from wide-ranging jet data. This definition describes the F404 maximum noise radiation angle from intermediate thrust through AB within 2°. Relating this expression to K-H Mach waves for an isothermal jet indicates the relative unimportance of temperature in determining maximum radiation angle for heated supersonic jets, including military jet aircraft and rockets.

## Nomenclature

$c_a$	= ambient sound speed, m/s
$c_j$	= fully expanded sound speed, m/s
$D_j$	= fully expanded diameter, m
$f$	= frequency, Hz
$M$	= convective Mach number (generic)
$M_{ac}$	= jet acoustic Mach number, $U_j/c_a$
$M_c$	= convective Mach number for the second family of instability waves; see Eqs. (3), (9), and (11)
$M'_c$	= convective Mach number for the first family of instability waves; see Eqs. (2), (8), and (10)
$M''_c$	= convective Mach number for the third family of instability waves; see Eq. (4)
$M_j$	= fully expanded Mach number, $U_j/c_j$
$M_O$	= Oertel convective Mach number
$M_{O\alpha}$	= convective amplification modification to $M_O$
OASPL	= overall sound pressure level, dB re 20 $\mu$ Pa
$St$	= Strouhal number, $fD_j/U_j$
$U_c$	= convective velocity, m/s
$U_j$	= fully expanded jet velocity, m/s
$w$	= velocity of the second (“supersonic instability”) family of instability waves, m/s
$w'$	= velocity of the first (“Kelvin–Helmholtz”) family of instability waves, m/s
$w''$	= velocity of the third (“subsonic instability”) family of instability waves, m/s
$\alpha$	= turbulent time to longitudinal scale ratio; see Eq. (14)
$\theta$	= angle relative to jet axis, deg
$\theta_M$	= maximum directivity angle derived from convective Mach number $M$ , deg; see Eq. (1)
$\theta_{max}$	= maximum observed noise directivity angle, deg

$\kappa$	= convective velocity coefficient, $U_c/U_j$
$\kappa(f)$	= frequency-dependent derived convective velocity coefficient
$\kappa_{OA}$	= overall derived convective velocity coefficient

## I. Introduction

SUPERSONIC jet noise is relevant to assessing impacts (e.g., hearing loss, annoyance, structural fatigue) from tactical aircraft, potential future commercial supersonic aircraft, and launch vehicles [1]. A detailed study of noise source and radiation characteristics across supersonic jet conditions improves physical understanding, resulting in better models of operational impacts and frameworks for noise reduction strategies. Important early studies involving supersonic jet noise included experiment reports by Westley and Lilley [2], Chobotov and Powell [3], Cole et al. [4], and Laufer [5] and analytical studies by Phillips [6] and Ffowcs Williams [7]. From these early studies came an understanding that supersonic jet noise radiation differed substantially from that of subsonic jets, including sound power increase with velocity, angle of maximum radiation, and spectral scaling. These early investigations spawned studies of supersonic jet noise radiation phenomena that continue today. Review papers on supersonic jet noise by Tam [8] and by Bailly and Fujii [9] elucidate several key findings, and Bailly and Fujii’s paper includes application to rockets, a topic reviewed in depth by Lubert et al. [10].

An important supersonic jet noise phenomenon is the relationship between the convection velocity  $U_c$  of large-scale turbulent structures and radiation angle. Beginning with Ffowcs Williams [7], who described an “eddy convective Mach number,” a convective Mach number has been used to describe the directivity of Mach wave radiation (MWR), typically seen as the dominant noise source in supersonic jets [11–15]. However, the calculation and interpretation of the convective Mach number have varied between researchers, with no one definition seeming to accurately predict the maximum radiation angle of all supersonic jets.

Using acoustic data and jet parameters from a T-7A-installed GE F404 engine, as well as from other sources, this paper discusses and compares physics-based and empirical definitions of the convective Mach number against measured far-field maximum directivity angles. The investigation significantly expands upon preliminary work by Christian and Gee [16]. First, different convective Mach numbers used previously to describe MWR are discussed in Sec. II. A description of the T-7A measurement is provided in Sec. III, along

Received 5 April 2024; revision received 20 September 2024; accepted for publication 4 November 2024; published online 29 November 2024. Copyright © 2024 by Kent L. Gee, Tyce W. Olaveson, and Logan T. Mathews. Published by the American Institute of Aeronautics and Astronautics, Inc., with permission. All requests for copying and permission to reprint should be submitted to CCC at [www.copyright.com](http://www.copyright.com); employ the eISSN 1533-385X to initiate your request. See also AIAA Rights and Permissions [www.aiaa.org/randp](http://www.aiaa.org/randp).

\*Professor of Physics, Department of Physics and Astronomy; [kentgee@byu.edu](mailto:kentgee@byu.edu). Associate Fellow AIAA (Corresponding Author).

<sup>†</sup>Graduate Student, Department of Physics and Astronomy. Student Member AIAA.

with key results needed for this paper's analysis and discussion: overall and frequency-dependent directivities and a holography-based source characterization. Using the definitions discussed in Sec. II, Sec. IV discusses the T-7A's physics-based and empirical convective Mach numbers for four engine conditions and compares predicted MWR angles with measurement. A frequency-dependent definition of convective Mach number for two T-7A engine powers is obtained from the frequency-dependent directivity curves. These results are placed in context with other supersonic jets, from laboratory-scale experiments through rockets. Using several laboratory-scale and rocket measurements, the relationship between convective velocity and jet acoustic Mach number is explored. This investigation results in a new definition for convective Mach number that appears to explain the maximum overall directivity angle across applicable supersonic jet conditions and agrees favorably with the T-7A data used as a validation. This new, data-derived convective Mach number is then analytically connected to a definition for Kelvin–Helmholtz (K-H) instability waves.

## II. Convective Mach Number Definitions

To the extent that a jet's directional radiation lobe is controlled by MWR, its maximum angle  $\theta_M$  is determined by the convective Mach number, referred to generically as  $M$ :

$$\theta_M = \cos^{-1}\left(\frac{1}{M}\right) \quad (1)$$

Although inlet angle is typically used for full-scale tactical jet noise descriptions, jet angle, which is measured from the jet centerline instead of from the aircraft's nose, is used in this paper given its topic and reference to laboratory, numerical, and tactical jets, as well as rocket plumes. Figure 1 describes the relevant anatomy of a supersonic jet with fully expanded jet exit velocity  $U_j$  and the Mach wave angle  $\theta_M$ .

### A. Oertel's Mach Numbers

Convective Mach numbers have typically been either physics-based or empirically derived. The physics-based definitions discussed here stem from the work of Oertel [17,18], who experimentally determined that Mach waves from a supersonic jet favor three distinct velocities,  $w' > w > w''$ . Though Oertel's work was initially empirical, Tam and Hu [19] followed up his work with analytical models that provided significant physical insight and suggested that these velocities are each associated with a type of instability wave. The first,  $w'$ , are the familiar K-H instability waves and have been associated with a strong acoustic field [19]. The second class of instability waves,  $w$ , are referred to by Tam and Hu as "supersonic instability waves." These waves have slower propagation speeds than the K-H instabilities, radiate at shallower angles, and may be related to Mach waves in supersonic,

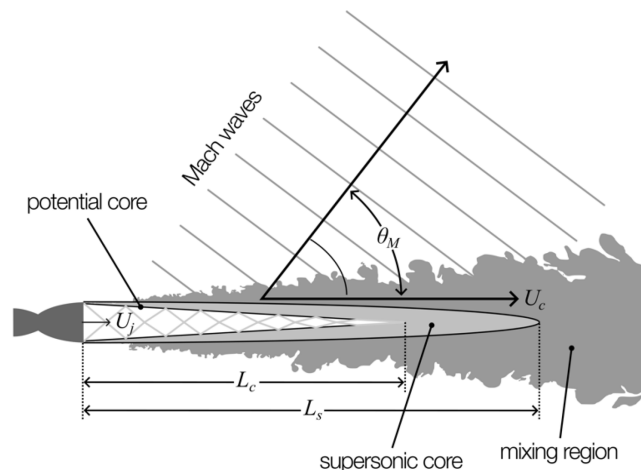


Fig. 1 Anatomy of a supersonic jet, with potential ( $L_c$ ) and supersonic ( $L_s$ ) core tips and Mach wave radiation.

turbulent shear layers. [20] The third family,  $w''$ , was referred to as subsonic instability waves by Tam and Hu [19] and decays rapidly in amplitude outside the jet. The physics of this family of waves has been studied in detail by Towne et al. [21] and by Nogueira et al. [22] in the context of potential core resonances and guided jet waves. They have shown that these instability waves are actually acoustic waves that see the shear layer of the jet as either a soft- or hard-walled duct, depending on frequency.

Oertel [17,18] expressed the convective Mach numbers for the three families of Mach waves as

$$M'_c = \frac{w'}{c_a} = \frac{M_j + 1}{1 + c_a/c_j} \quad (2)$$

$$M_c = \frac{w}{c_a} = \frac{M_j}{1 + c_a/c_j} \quad (3)$$

and

$$M''_c = \frac{w''}{c_a} = \frac{M_j - 1}{1 + c_a/c_j} \quad (4)$$

where  $M_j$  and  $c_j$  represent fully expanded Mach number and sound speed, respectively, and  $c_a$  represents the ambient sound speed. Correspondingly, thresholds for their existence as radiated Mach waves may be written as

$$w' > c_a \quad \text{for } M_j > c_a/c_j \quad (5)$$

$$w > c_a \quad \text{for } M_j > 1 + c_a/c_j \quad (6)$$

and

$$w'' > c_a \quad \text{for } M_j > 2 + c_a/c_j \quad (7)$$

Equations (5) and (6) say that the K-H  $w'$  and supersonic instability (SI)  $w$  Mach waves are convectively supersonic when the fully expanded Mach number exceeds thresholds based on the ratio of the ambient and fully expanded jet sound speeds,  $c_a/c_j$ . This is also true of  $w''$  (subsonic instability waves) in Eq. (7); however, their rapid amplitude decay outside the jet boundary indicates that they are unlikely to contribute significantly [23] to the noise, even when convectively supersonic. Because this class of waves does not result in strong MWR, the K-H and SI waves are the focus of this paper. Before proceeding, however, we note that Oertel et al. [24] proposed an alternate physical interpretation than Tam and Hu [19] for the Mach wave families. The theory describes the creation of paired vortices by the rolling up of K-H waves, but the convective Mach number expressions do not match those previously shown by Oertel [17,18] to agree remarkably well with the experiment. Because this later paper has begun to be cited in place of Oertel's earlier works, we caution against its quantitative use without further, corroborative investigations.

Oertel's convective Mach number expressions in Eqs. (2–4) are expressed in terms of  $M_j$  and the ratio  $c_a/c_j$ , whereas Seiner et al. [23] and many authors since have opted to write them simply in terms of velocities. These alternative expressions for the K-H and SI wave families of convective Mach numbers are written as

$$M'_c = \frac{U_j + c_j}{c_j + c_a} \quad (8)$$

and

$$M_c = \frac{U_j}{c_j + c_a} \quad (9)$$

One possible advantage with Eqs. (8) and (9) over Eqs. (2) and (3) is that it is simpler to understand when these Mach waves radiate. For

example, the SI Mach waves radiate noise whenever the jet velocity is greater than the sum of the jet and ambient sound speeds [23]. They are also intermediate to a third form of these expressions that is useful to later discussion in this paper and which can be found by multiplying the numerator and denominator of Eqs. (8) and (9) by  $1/c_a$ . This operation results in

$$M'_c = \frac{M_{ac} + c_j/c_a}{1 + c_j/c_a} \quad (10)$$

and

$$M_c = \frac{M_{ac}}{1 + c_j/c_a} \quad (11)$$

where  $M_{ac}$  is the jet acoustic Mach number,  $U_j/c_a$ . These latter forms of the convective Mach numbers for the K-H and SI waves are useful for two reasons. First, by using  $M_{ac}$  they can be directly connected to empirical definitions of convective Mach number. Second, they invert the  $c_a/c_j$  relationship employed in Oertel's works and by Tam and Hu [19], resulting in the ratio  $c_j/c_a$  as the parameter that describes the role of temperature in determining convective Mach number. Although rewriting the thresholds for MWR in Eqs. (5) and (6) in terms of  $c_j/c_a$  is analytically inelegant, we prefer the use of this ratio because with increasing military jet engine power (like the T-7A case considered here) and in the transition from jet to rocket noise,  $c_j/c_a$  and  $M_{ac}$  jointly increase.

It is instructive to observe the predicted Mach wave angle stemming from  $M'_c$  and  $M_c$  as a function of  $M_j$  for different values of  $c_j/c_a$ . Figure 2a shows the Mach wave angle  $\theta_M$  (see Fig. 1 for its definition) for  $M'_c$  (solid lines) and  $M_c$  (dashed lines) as a function of  $M_j$  over a range of values from 1 to 4, which contains typical fully expanded Mach numbers of tactical jet aircraft and rockets. Different cases of  $c_j/c_a$  are shown, including for the T-7A at military (MIL) and afterburner (AB) engine powers and a typical value for a rocket. Note first that a nonzero  $\theta_{M'_c}$  at  $M_j = 1$  shows that K-H Mach waves can exist for highly heated, subsonic jets. Second, as  $c_j/c_a$  increases, the  $M_j$  at which  $M_c$  becomes supersonic lessens. Because the theory

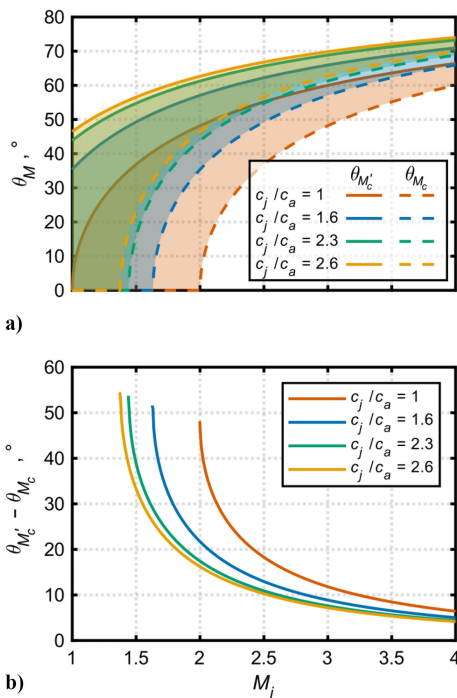


**Fig. 2** a) Predicted radiation angle for  $M'_c$  and  $M_c$  as a function of  $M_j$ . Different  $c_j/c_a$  are shown, including those of the T-7A at military and AB engine powers and a typical rocket value. b) Difference in  $M'_c$  and  $M_c$  radiation angle.

of Tam and Hu indicates an eventual merger of the K-H and SI Mach waves as  $M_j$  and  $c_j/c_a$  increase, Fig. 2b shows the difference in the radiation angles of the two classes of Mach waves. At AB and rocket-like sound-speed conditions, the two waves are separated by  $10^\circ$  at slightly more than  $M_j = 2.5$ , with likely significant overlap between radiation lobes. By  $M_j = 4$ , the radiation angle difference is only  $\sim 5^\circ$  for any heated jet.

Despite the work of Oertel, the impact of the K-H and SI waves on the radiated far-field acoustics has been left unclear. Many supersonic jets studied do not reach sufficient velocities and temperatures to have SI waves present. Furthermore, they may radiate at shallow angles, where distinguishing them from the “large-scale” noise present for both subsonic and supersonic jets in that region can be difficult. A literature search for cases with sufficiently large K-H and SI amplitudes and clear separation has uncovered two illustrative examples, which have been digitized [25] from plots in their respective papers. They are shown here to illustrate the differences in K-H and SI radiation efficiency and angles. First, in Seiner et al.'s [23] classic study of Mach wave phenomena, they kept their ideally expanded jet at  $M_j = 2.0$  and increased temperature, i.e.,  $c_j/c_a$ . The far-field overall sound pressure levels (OASPL) for their highest temperature condition ( $c_j = 591$  m/s) are shown in Fig. 3a. The graph is annotated with the calculated angles for both K-H and SI Mach waves, and there are clear maxima around these regions. Evidence of the SI wave in the OASPL for the lesser temperature jets measured by Seiner et al. is less clear. The second example, in Fig. 3b, is the Mach 3.0 unheated ( $c_j = 204$  m/s) jet studied by Baars [26] and Baars et al. [27]. In this case, the OASPL contour plot was digitized to create a surface used to extract levels along the  $100 D_j$  arc centered at a microphone array reference point (MARP) located at  $17.5 D_j$  downstream of the nozzle exit. The data again show two maxima in the vicinity of the two Mach angles. This assertion is strengthened by examination of a large-eddy simulation by Pineau and Bogey [28] at the same conditions of the Baars et al.'s jet. Their Fig. 1 shows Mach waves radiating around both the angles indicated in Fig. 3b, although a slight peak in the OASPL pattern around  $27^\circ$  in their Fig. 4 is not as pronounced as in Fig. 3b. Nonetheless, these two supersonic jet measurement

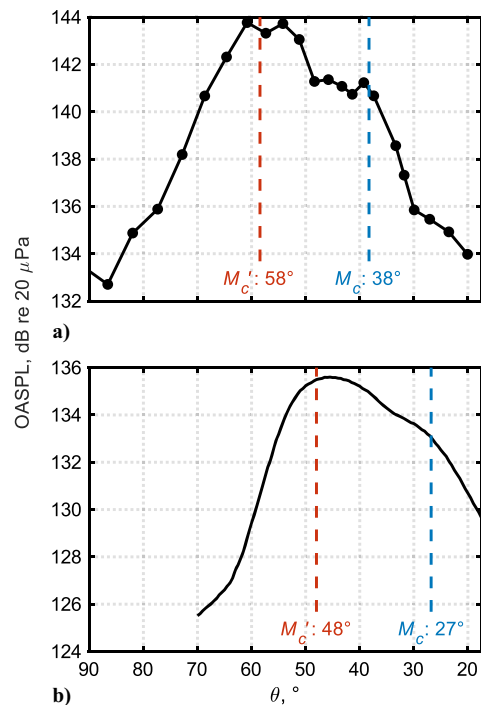
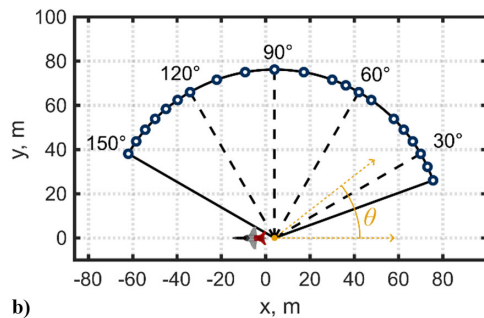


**Fig. 3** Overall sound pressure level (OASPL) as a function of jet angle for two supersonic jets, annotated with the calculated  $M'_c$  and  $M_c$ . a) Seiner et al.'s  $M_j = 2.0$ ,  $c_j/c_a = 1.74$  jet at a common corrected distance of  $40 D_j$  [23]. b) Baars et al.'s  $M_j = 3.0$ ,  $c_j/c_a = 0.594$  jet at  $100 D_j$  [26,27].



a)



b)

**Fig. 4** a) Tied-down T-7A facing the jet blast deflector, with microphone stands in the foreground. b) Schematic of aircraft and 76 m microphone array with MARP 4 m downstream of the nozzle.

examples help to elucidate the overall level directivity patterns expected from the Oertel [17,18] and Tam and Hu [19] convective Mach number theory in the regime where both K-H and SI waves are present for non-rocket-like conditions.

### B. Oertel Convective Mach Number

Oertel's physics-based investigations spawned related semi-empirical formulations for the convective Mach number. In studies of jet noise radiation across different conditions, from laboratory-scale jets through rockets, Greska [29] and Greska et al. [30] linked the maximum overall noise radiation to the K-H and SI waves, Eqs. (8) and (9), by taking their arithmetic mean. This new parameter, dubbed the "Oertel convective Mach number"  $M_O$ , in honor of Oertel, is typically written as

$$M_O = \frac{M'_c + M_c}{2} = \frac{U_j + (1/2)c_j}{c_j + c_a} \quad (12)$$

(To clarify any potential for confusion, some authors, e.g., the authors of Refs. [29–32], have previously called  $M'_c$  in Eq. (8) the Oertel convective Mach number or the maximum Oertel convective Mach number.) Aside from being motivated by better data collapse in Ref. [29], a physical basis for averaging these two Mach numbers stems from Greska noting that two conditions seemed to occur concurrently for the jets studied. First, Mach waves are described as fully developed and readily identified in the jet noise for  $M'_c > 1.25$ , [13,31], although Kearney-Fischer et al. [12] suggest that this threshold should be treated as only a rough guide based on the limited range of jet conditions originally studied [31]. Second, the normalized shear layer growth becomes constant for  $M_c > 0.8$ . Justification for the use of  $M_O$  as a physics-based convective Mach number definition for rocket-like jet conditions (where  $M'_c$  and  $M_c$  are both well above their onset thresholds; see Fig. 2) has been provided by Langenais et al. [35], who found that a large-eddy simulation produced structures that propagated at the average of  $M_c$  and  $M'_c$ . At this jet condition, however, the two Mach wave angles are only separated by about  $8^\circ$ , suggesting the possibility of significant overlap in radiation from the K-H and SI waves. Nonetheless, this work by Langenais et al. helps to explain the success of

the Oertel convective Mach number as defined in Eq. (12) in predicting maximum directivity angles from rocket static firing and launch measurements. James et al. [36], Hart et al. [37], Bassett et al. [38], and Lubert et al. [10] each showed that  $M_O$  predicted the far-field  $\theta_{\max}$  of different rockets within just a couple of degrees.

Although  $M_O$  works to predict the maximum directivity angle for rocket-like conditions because of the convergence of  $M'_c$  and  $M_c$  radiation angles (see Fig. 2b), it does not work for all jet conditions. Greska [29] discussed how neither  $M'_c$  nor  $M_O$  as defined in Eq. (12) predicted the measured  $\theta_{\max}$  for the jets studied. He turned to Ffowkes Williams's [7] theory of convective amplification to propose a modification to  $M_O$ , which we refer to as  $M_{O\alpha}$ . This modified Oertel convective Mach number is expressed as

$$M_{O\alpha} = M_O[1 + \alpha^2 - (\alpha\epsilon)^2] \quad (13)$$

where  $\alpha$  is the ratio of the turbulent time to longitudinal scales, defined by Greska after investigation of his data as

$$\alpha = -0.4M_j + 1.1 \quad (14)$$

and  $\epsilon$  is the ratio of the turbulent longitudinal to lateral scales, assumed by Greska as fixed at  $\epsilon = 0.33$ . Note that  $\alpha$  becomes negative for  $M_j > 2.75$  in Eq. (14), meaning that this expression cannot be physical for rockets, despite the fact that Eq. (13) only involves the use of  $\alpha^2$ . Thus, this convective amplification-modified form of  $M_O$  at present is an empirical correction derived from a range of laboratory jet conditions.

### C. Empirically Derived Convective Velocity

Stepping aside from the theoretical models used to predict convective velocities, many jet aeroacoustics studies have used an empirical definition for the convective Mach number based on  $U_c$  being some fraction of the fully expanded centerline velocity  $U_j$ . This ratio, defined here as  $\kappa = U_c/U_j$ , results in the following definition of convective Mach number:

$$M_\kappa = \frac{U_c}{c_a} = \frac{\kappa U_j}{c_a} = \kappa M_{ac} \quad (15)$$

Determining  $\kappa$  has been the goal of some studies, while others have assumed a value for  $\kappa$  in modeling and related work without explicit rationale, other than it falls within a "typical" range. In actuality, values for  $\kappa$  vary with jet conditions. For example, several studies have shown a reduction in convective velocity for increased temperature [39–42]. Additionally, for a range of laboratory-scale and simulated supersonic jets, researchers have suggested  $\kappa$  values associated with the peak overall radiation (hereafter explicitly referred to as  $\kappa_{OA}$ ) between 0.6 and 0.85 for various jet parameters [23,26, 42–45], while rocket noise research has shown values closer to 0.3 are more appropriate [10,37,38,46]. However, there does not seem to be an explicit relation for  $\kappa_{OA}$ , empirical or otherwise, that spans all heated supersonic jet conditions and describes the far-field maximum directivity angle.

Furthermore,  $\kappa$  should vary across frequency [hereafter explicitly denoting frequency-dependence as  $\kappa(f)$ ], given its dependence on  $U_j$ , the slowing of the convectively supersonic jet after the end of potential core tip, and downstream shift of noise source location with decreasing frequency. However, there are relatively few studies that have investigated this phenomenon. Of note are Morris [47], Neilsen et al. [48], and Baars et al. [49]. Morris and Neilsen et al. both used similarity-spectrum-educed wavepacket models to obtain wavenumber spectra and determine an effective  $U_c$ . While Morris found a 15% increase in  $\kappa(f)$  with frequency across  $0.05 < Sr < 0.4$  for a Mach 1.8 jet with a temperature ratio of 1.65 and an average value of  $\kappa_{OA} \approx 0.6$ , Neilsen et al. found that an unheated Mach 1.8 jet resulted in a relatively constant  $\kappa(f) \approx 0.8$  from  $0.2 < Sr < 2$ , but only after a frequency-dependent source origin was considered. Baars et al. [49] also considered a frequency-dependent source origin in their study of a Mach 1.55 jet with a temperature ratio of 3.47, and they found that

$\kappa(f)$  was greater than 0.65 for  $Sr > 0.2$  but then decreased to 0.5 at  $Sr \approx 0.05$ , with an additional bump in  $\kappa(f)$  at  $Sr \approx 0.6$ . Both a broadly applicable relationship for  $\kappa_{OA}$  and an exploration of its frequency dependence  $\kappa(f)$  using T-7A data are explored in Sec. IV.

### III. T-7A Measurement

#### A. Measurement Setup

The Boeing/Saab T-7A “Red Hawk” supersonic trainer aircraft is powered by a single F404-GE-103 jet engine. The F404 engine has previously been the subject of noise characterization and reduction studies [50–57]. As described in Ref. [58], acoustical measurements were made of a T-7A-installed F404 engine at Holloman Air Force Base in 2019 at the same run-up pad used previously for F-22 measurements [59]. However, as seen in Fig. 4, the tied-down aircraft was uniquely oriented with the nose toward the closest jet blast deflector to have an undeflected jet over a greater distance (~60 m) than otherwise possible. The aircraft was then cycled through six engine powers from idle to AB, with the aircraft held at each condition for 30 s. Jet parameters were obtained at each of these conditions using the Numerical Propulsion System Simulation (NPSS<sup>®</sup>) software [60] run for the measurement ambient conditions. While the uncertainty between actual measured exhaust conditions and those estimated via NPSS is not presently able to be evaluated, the code was run in excess of 100 times for each engine condition, and the standard deviation for the parameters was less than 2% for all engine conditions. This paper includes analyses of the four highest engine powers measured: 38% thrust, 55% thrust, military power (MIL), and AB. (Note that the 38 and 55% thrust conditions are the same as slightly different values reported by Christian et al. [61].) For 38% thrust,  $M_j < 1$ , whereas it is supersonic for the other conditions. Although the run-up cycle was completed six times, the far-field data for the first two run-ups varied because of a predawn temperature inversion [62]. Consequently, the levels and spectra for the last four run-ups, obtained from Hann-windowed 1 s blocks with 50% overlap over the 30 s recording, are averaged and used in this study.

As described in Refs. [50,58], the measurement consisted of over 200 microphones arranged in both the geometric near and far fields. This paper focuses on just the far-field arc at 76 m (250 ft), which had 22¼” GRAS 46BD microphones sampled at 96 kHz using 24-bit NI<sup>®</sup> PXI-4496 data acquisition cards. Per the relevant ANSI standard [63], microphones were placed relative to the MARP, located 4 m (13 ft) downstream of the nozzle or approximately 7–8 nozzle diameters. Although inlet angles are typically used with full-scale jet noise studies, this paper uses jet or laboratory angles because of their natural tie to Mach waves and easy comparison against laboratory-scale and rocket data. As seen in Fig. 4, the 76-m-arc microphones were located from 20 to 150° in 5° increments from 20 to 70° and from 120 to 150°, and a 10° resolution elsewhere; the

uncertainty in microphone placement is  $\pm 0.25^\circ$ . A loose cable connection resulted in unusable data at 50°; they are excluded from analysis.

The 76 m microphones were located at a height of  $1.5 \pm 0.03$  m (5 ft  $\pm 1$  in.) above the ground, resulting in multipath interference effects in the measured spectra. Christian et al. [64] have discussed these effects’ reasonable removal through a ground reflection model [65] that accounts for source and receiver geometry, source extent and correlation, a finite-impedance ground, and a turbulent atmosphere. In addition to the analysis here, this model was also used recently in an F404 sound power and acoustic efficiency investigation [61].

#### B. Directivity Results

Figure 5 shows the average OASPL directivity curves generated from the T-7A data at the four engine conditions considered. The markers represent the levels measured by the mics, while the lines connecting them are interpolated using a shape-preserving piecewise cubic interpolation method. Shaded regions around each curve indicate the maximum and minimum OASPL values among each of the four run-ups. There is little variation around in the primary radiation direction, with less than a 0.5 dB difference from the mean. Both the forward and shallow angles exhibit broader ranges but are not the focus of this study. Note that the maximum radiation angle increases from ~30 to ~60° as the engine power increases from 38% to AB, with a radiation lobe widening that is usually attributed to increased temperature. The width of the 3-dB-down (full-width-half-maximum) lobe at AB is ~35°, similar to that seen for an afterburning F-35 [66] and for a launched Falcon 9 [46]. Also of note is the saturation in mean sound levels from 20 to 35° in the transition from MIL to AB. A similar phenomenon occurred with the F-35 over the same angular range (inlet angles of 145–160°) [66], suggesting that different source mechanisms are controlling the radiation for high-power tactical jet aircraft in the far aft region than the maximum MWR-controlled region that continues to shift to greater jet angles and amplitudes as jet velocity and temperature increase.

In Fig. 6, the MIL and AB OASPL directivity curves from Fig. 5 are repeated and shown along with several one-third octave (OTO) band directivity patterns scaled in terms of Strouhal number,  $Sr = fD_j/U_j$ . At the lowest frequency,  $Sr = 0.01$ , the radiation peaks for both MIL and AB appear at about 30°, with the peak for AB being slightly forward. At  $Sr = 0.06$ , the relative radiation at AB is 3–4 dB greater than at MIL, with the angle shifting forward by about ~7°. At  $Sr \approx 0.25$ , the peak noise level is approximately the same at around 120 dB re 20  $\mu$ Pa at 76 m, but has shifted from 55 to 65° in going from MIL to AB. This shift appears to be responsible for the flatter OASPL directivity for AB, with radiation at angles greater than 60°. For both engine conditions, higher frequencies ( $Sr \approx 5$  and 10) continue to radiate in approximately the same direction (55–60° for MIL and

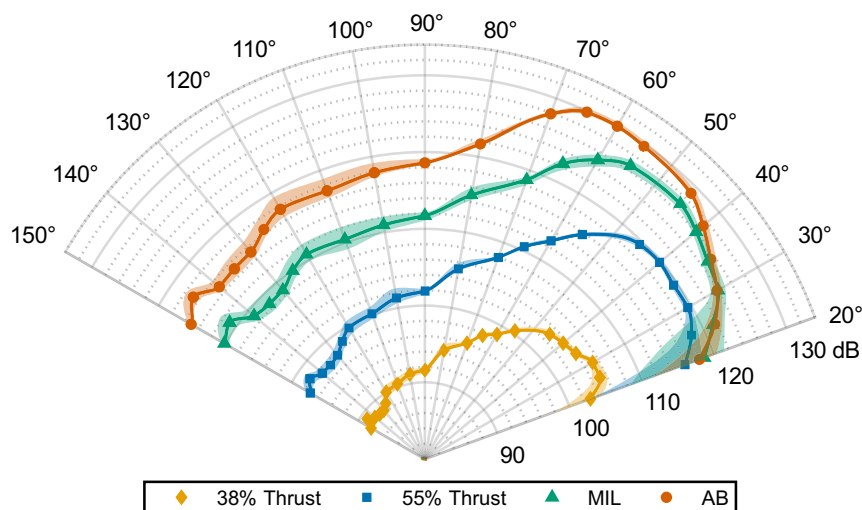


Fig. 5 T-7A OASPL directivity curves at the 76 m arc for the four highest engine conditions measured.

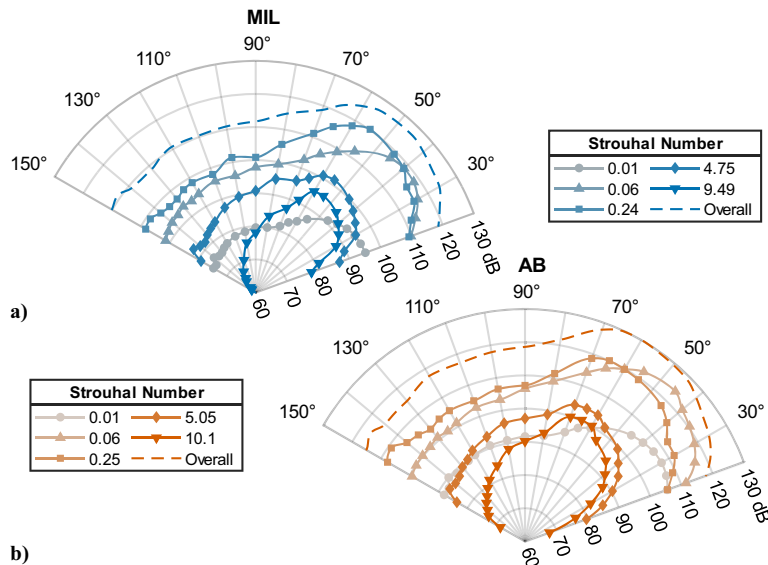


Fig. 6 T-7A overall (OASPL) and one-third octave band directivity curves at the 76 m arc for a) MIL and b) AB.

$\sim 65^\circ$  for AB) with progressively narrower lobes. A similar phenomenon was seen for the F-35 at MIL and AB (see Fig. 14 in Ref. [66]), with the directivity angles for the highest frequencies shown matching the T-7A quite well. This consistency in radiation lobe maximum direction and progressive narrowing with increasing frequency may be the unidirectionality of MWR upstream of the potential core tip,  $L_c$  [67], or perhaps it could be the result of nonlinear acoustic propagation, which is most concentrated around the maximum OASPL angles. A similar narrowing was seen in rocket booster directivity measurements [68]. In any event, however, the angle shift forward over a frequency range implies that  $\kappa$  in Eq. (15) changes as a function of frequency.

### C. Aeroacoustic Source Location

The third T-7A measurement and analysis result that is important to the subsequent convective Mach number analysis is a description of the dominant aeroacoustic source region as a function of frequency. Figure 7 shows a spatio-spectral map for normalized sound pressure level along the T-7A nozzle lipline at AB, generated using a near-field acoustical holography-based reconstruction [69]. This reconstruction describes the apparent aeroacoustic source region as

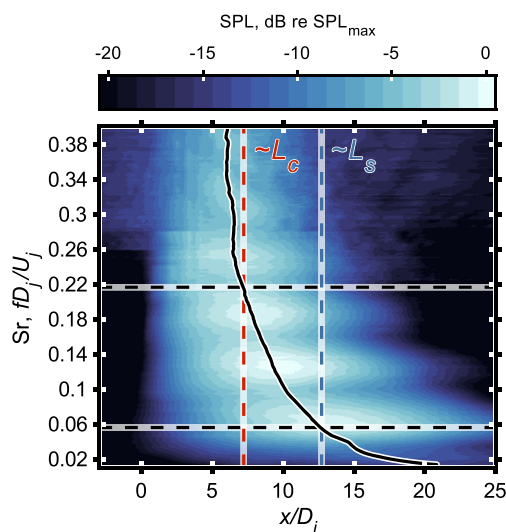


Fig. 7 Spatio-spectral map from an apparent source near-field acoustical holography field reconstruction [69]. The black line shows the maximum level at each  $Sr$  and the dashed lines show where the maximum  $Sr$  intercepts  $L_c$  and  $L_s$ , the potential and supersonic core length, respectively.

a function of  $Sr$  and scaled downstream distance,  $x/D_j$ . Also shown on the map are lines corresponding to the approximate potential ( $L_c \sim 7.2D_j$ ) and supersonic ( $L_s \sim 12.7D_j$ ) core lengths (see Fig. 1), as obtained from a large-eddy simulation of a highly heated supersonic jet with conditions similar to AB [11] and justified in a literature review by Mathews et al. [70]. Tracing the source maximum location as a function of  $Sr$  (black line in Fig. 7) and determining its intercept with  $L_c$  and  $L_s$  results in estimates for the peak frequencies originating from these two locations. At  $L_c$ , the peak  $Sr$  appears to be  $\sim 0.22$ ; at  $L_s$ , the peak  $Sr$  is  $\sim 0.06$ . In the subsequent analysis examining  $\kappa(f)$  in Sec. IV.B, this discussion of the results in Fig. 7 is essential to its interpretation.

## IV. Convective Mach Number Analysis

This section contains various convective Mach number analyses using the T-7A measurement and holography-derived data discussed in Sec. III. Section IV.A contains analyses of the overall directivity, whereas Sec. IV.B describes a frequency-dependent  $\kappa(f)$ . Finally, Sec. IV.C returns to the concept of  $\kappa$  for overall directivity but connects it to the jet condition and to Oertel's work. The analysis yields a new definition of convective Mach number that only requires knowledge of  $U_j$  and  $c_a$  and appears to predict  $\theta_{\max}$  with reasonable fidelity from laboratory-scale supersonic jets through rockets.

### A. T-7A Convective Mach Number Calculations

Table 1 lists scaled engine parameters obtained for different definitions of the convective Mach number using the T-7A data at different engine powers. The convectively supersonic Mach numbers are then used to predict a peak radiation angle using Eq. (1). These predicted angles, given in parentheses next to their accompanying convective Mach number, may be compared against  $\theta_{\max}$ . To obtain a more precise angle estimate than the  $5^\circ$  maximum measured resolution, a cubic polynomial was fit to the top 3 dB of each OASPL directivity function. Table 1 also shows the values for  $\kappa_{OA}$  calculated from the measured  $\theta_{\max}$  using the relation

$$\kappa_{OA} = \frac{c_a}{U_j \cos(\theta_{\max})} \quad (16)$$

One of the most significant findings from Table 1 is that, while  $M'_c$  matches  $\theta_{\max}$  for all four engine conditions to within  $5^\circ$  ( $2^\circ$  for non-afterburning conditions),  $M_c$  is subsonic until AB, where it reaches a value of  $M_c = 1.01$ . This indicates that the noise radiation for all supersonic engine conditions is dominated by K-H MWR and the SI waves do not factor in—a perhaps surprising conclusion of this paper.

**Table 1** Calculated convective Mach number values and their predicted angles from T-7A data compared against the measured peak radiation angle, relative to an origin 4 m from the nozzle exit

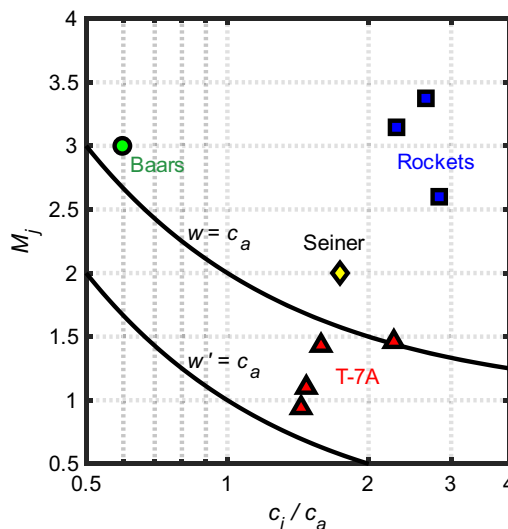
Condition	$M_j$	$M_{ac}$	$c_j/c_a$	$\theta_{max}$	$M'_c(\theta_{M'_c})$	$M_c(\theta_{M_c})$	$M_O(\theta_{M_O})$	$M_{Oa}(\theta_{M_{Oa}})$	$\kappa_{OA}$
38%	0.94	1.35	1.44	28°	1.14 (29°)	0.55 (—)	0.85 (—)	1.25 (37°)	0.84
55%	1.10	1.62	1.47	39°	1.25 (37°)	0.66 (—)	0.95 (—)	1.32 (41°)	0.79
MIL	1.43	2.27	1.58	49°	1.49 (48°)	0.88 (—)	1.18 (32°)	1.48 (47°)	0.67
AB	1.46	3.30	2.26	59°	1.70 (54°)	1.01 (9°)	1.36 (43°)	1.68 (53°)	0.59

Examining the details more closely,  $M'_c$  is supersonic for all four engine conditions, even though the engine exhaust is subsonic at 38% thrust. This may be evidence of MWR from a heated subsonic jet. However,  $\theta_{max} = 28^\circ$  is similar to the  $\sim 30^\circ$  maximum radiation angle typically seen for heated, subsonic jets, and it is below the  $M'_c = 1.25$  suggested threshold. Furthermore, Christian et al. [61] found that the sound power radiation transition between 17 and 38% thrust for the F404 engine closely approximates the subsonic  $U_j^8$  law [71]. Thus, the actual role of MWR is unclear for 38% thrust. Between 38 and 55% thrust, however,  $M_j$  exceeds 1, there is a jump in acoustic efficiency [61], and the  $M'_c = 1.25$  threshold is reached. The practical consequence of these changes is that  $\theta_{max}$  increases to  $39^\circ$  ( $M'_c$  prediction is  $37^\circ$ ), and the radiation lobe widens such that there is nearly uniform OASPL between  $30$  and  $50^\circ$ . For MIL,  $\theta_{max}$  moves to  $49^\circ$  as the lobe width continues to widen and  $M'_c$  again closely predicts this angle.

For AB, the  $5^\circ$  disagreement between  $\theta_{max}$  and the  $M'_c$  angle, if considered meaningful given the near-perfect lobe flatness, appears to be caused by an enhancement in radiation around  $65^\circ$  ( $115^\circ$  inlet angle) that continues to flatten the OASPL lobe and pushes the T-7A's overall directivity lobe forward. An examination of Fig. 6 shows that the peak directivity angle is  $65^\circ$  for frequency around  $Sr = 0.25$  and higher. Figure 7 and additional holography on an AB-like large-eddy simulation [72] indicate that, for  $Sr > 0.25$ , the noise at AB originates at or upstream of  $L_c$ . MWR in the  $60$ – $70^\circ$  range has been studied for the T-7A [73,74] and for the F-35 [67,75]. The radiation at these angles, which is linked to spatio-spectral lobes present in the noise field [73–75], appears to originate from turbulent structures with convective Mach numbers greater than  $M'_c$ . Given that shock cells result in local plume velocities that exceed  $U_j$  (e.g., see Refs. [35,72] for simulation examples), convective velocities that appear greater than those allowed by K-H waves based on  $U_j$  may strengthen prior assertions [76,77] that shock cells are directly connected to the presence of spatio-spectral lobes. Conversely, there is no possibility that the spatio-spectral lobes, which exist at multiple engine conditions, are simply manifestations of Oertel's multiple classes of Mach waves because SI waves do not radiate for the T-7A at non-afterburning conditions. Furthermore, at AB,  $M_c$  is so low that it would not contribute meaningfully to the observed OASPL radiation lobe.

Referring to Greska's Mach number definitions, the reason for the failure of  $M_O$  to predict radiation angle for T-7A conditions in Table 1 is made clear, as the SI is nonexistent or unimportant to the radiation. However, an examination of  $M_{Oa}$  [29] reveals that the convective amplification term and data-derived definition of  $\alpha$  in Eq. (14) seem to function acceptably well to correct  $M_O$  for the higher T-7A engine powers. However, Greska's motivation for pursuing the development of  $M_{Oa}$  does not hold in the case of the T-7A data, whereas  $M'_c$  did not adequately predict  $\theta_{max}$  for the jets he studied and  $M_{Oa}$  performed better, neither is the case for the T-7A data; the K-H wave-based definition of convective Mach number provides as good or better agreement with the observed far-field  $\theta_{max}$ .

Figure 8 contextualizes the T-7A convective Mach numbers and directivity angles in Table 1 relative to the Oertel Mach waves and other supersonic jets. The plot shows the  $M_j$  thresholds for the existence of the three classes of Mach waves from Eqs. (5–7), expressed as a function of  $c_j/c_a$ . The T-7A data are shown as triangles, with AB just barely exceeding the threshold for the existence of  $w'$  waves. For the sake of comparison, the jets of Seiner et al. [23] and Baars et al. [26,27] discussed in conjunction with Fig. 3 are

**Fig. 8** Threshold curves for onset of K-H and SI Mach wave radiation at a given  $M_j$  as a function of  $c_j/c_a$ , along with T-7A engine powers. The  $M_j = 2.0$  Seiner jet, the  $M_j = 3.0$  Baars jet, and rockets are shown for the sake of discussion.

also shown. They are sufficiently removed from the  $w$  threshold that their SI wave radiation begins to appear in the vicinity of the principal radiation lobe. Shown also are three rocket data points, corresponding to Refs. [13,37,38], to demonstrate how far removed they are from the K-H and SI wave boundaries. The locations of the rocket data points relative to the  $w$  and  $w'$  thresholds also mean that their lobes have significant overlap and the use of  $M_O$  to predict  $\theta_{max}$  is appropriate.

As a final note regarding definitions of convective Mach number and the T-7A data, the far-right column of Table 1 shows the overall convective velocity fraction,  $\kappa_{OA}$ , for all four engine conditions as calculated from Eq. (16). As expected based on increasing temperature,  $\kappa_{OA}$  decreases with engine power. It is interesting that the values span those seen in the literature,  $\sim 0.6$  to  $0.8$ . This helps to connect the T-7A conditions to prior literature that has either calculated using different methods for  $\kappa_{OA}$  or assumed a value. However, it is shown in Sec. IV.C that empirical estimates for convection velocity fraction are no longer necessary, based on a simple relationship that provides accurate predictions for an OASPL-based  $\theta_{max}$  over relevant supersonic jet conditions.

## B. Frequency-Dependent Effects

As discussed in Sec. II.C, given the change in jet and convective velocity with distance downstream,  $\kappa$  is frequency-dependent; for clarity, we refer to the frequency-dependent parameter as  $\kappa(f)$ . To improve understanding of this relationship, Fig. 9 shows  $\kappa(f)$  as a function of  $Sr$  for the T-7A at both MIL and AB conditions. These  $\kappa(f)$  values were obtained by obtaining each OTO directivity pattern (e.g., see Fig. 6), finding the maximum radiation angle using a cubic polynomial of the top 3 dB of the curve, and then using Eq. (16). The same process was completed with narrowband spectra; the only impact of using OTO spectra is data smoothing; there is no meaningful loss of information, particularly given the  $5^\circ$  measurement resolution. In Fig. 9, vertical lines represent the frequencies whose

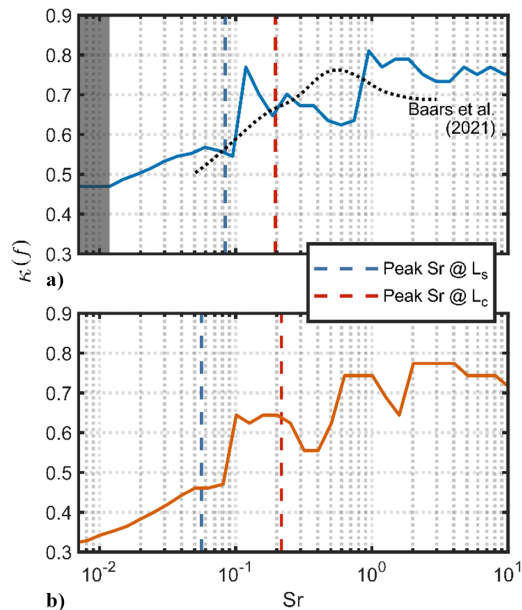


**Fig. 9** The  $\kappa(f)$  values as a function of  $Sr$ , calculated from frequency-dependent peak directivity angles at a) MIL and b) AB. The MIL data are compared against similar data from Baars et al. [49].

maximum source locations correspond to  $L_c$  (red dashed line) and  $L_s$  (blue dashed line), as obtained through acoustical holography. (An example for AB was shown previously in Fig. 7.) In Fig. 9a, the shaded area represents the frequencies for which the maximum angle is  $\leq 20^\circ$ , and  $\kappa(f)$  cannot be accurately determined. Because Fig. 9a represents MIL power and is fairly close to the conditions of Baars et al. [49], their data are shown over their calculated range of  $Sr$  values. For the data of Baars et al., their values range between 0.5 and 0.77, with the peak around  $Sr \approx 0.55$  and an apparent convergence at high frequencies to  $\kappa(f) \approx 0.7$ . The T-7A extraction data are noisier, possibly in part from some residual ground-reflection effect that causes spectral ripples, but range from  $\kappa(f) \approx 0.5$  at low frequencies with a downward slope to a convergence to  $\kappa(f) \approx 0.77$  at high frequencies. For AB in Fig. 9b, the  $\kappa(f)$  values start out lower, near 0.3, at the lowest frequencies, before increasing to a high-frequency value of  $\kappa(f) \approx 0.75$ . For both conditions,  $\kappa(f)$  increases rapidly for frequencies whose locus occurs just upstream of  $L_s$  and then increases (with noise) more slowly for frequencies that originate upstream of  $L_c$ . Conceptually, this behavior for  $\kappa(f)$  fits with the interpretation of MWR proffered by Vaughn et al. [67] (see their Fig. 10d) using an event-based beamforming method and Leete et al. [78] (see their Fig. 6b) using a frequency-averaged coherence analysis. In both cases, unidirectional radiation was observed upstream of  $L_c$  (represented by the high-frequency flattening of  $\kappa(f)$ ), a shift to lesser angles corresponding to convectively supersonic radiation with slowing velocities between  $L_c$  and  $L_s$  (represented by the relatively sharp transition in  $\kappa(f)$ ) and then a termination of the dominant radiation to shallow angles within a few nozzle diameters beyond  $L_s$  (a transition to low  $\kappa(f)$  values).

### C. Physics-Based, Data-Driven Expression for Convective Mach Number

As discussed in Sec. II.C, a drawback of the empirical definition  $M_\kappa$ , given in Eq. (15), is the varied values of  $\kappa_{OA}$  given by different authors without clear underlying physical justification, which may impact conclusions and make comparisons difficult. To summarize, supersonic laboratory jets and numerical simulations have found or assumed  $\kappa_{OA}$  to be within  $\sim 0.6$  and  $\sim 0.85$ , with some studies observing a decrease with temperature, but closer to  $\kappa_{OA} \approx 0.3$  for rocket conditions. Because velocities and temperatures from rockets are both significantly greater than those seen in laboratory-scale jets and tactical engines, whether the variability in  $\kappa_{OA}$  is due to the increase in velocity or temperature is not well understood. However,

investigation [16] into these changes using data from several studies has revealed that the change in  $\kappa_{OA}$  is most strongly correlated with  $M_{ac}$ , less so with temperature ratio, and not hardly at all with  $M_j$ . Consequently, a more detailed investigation into the relationship between  $\kappa_{OA}$  and  $M_{ac}$  has been carried out. Using reported  $\theta_{max}$  and jet parameters from laboratory jets [12,23,26,29,49,79–81], numerical simulations [35,42,72],<sup>‡</sup> and rockets [13,36,37,46],  $\kappa_{OA}$  has been determined using Eq. (16) as a function of  $M_{ac}$ . The T-7A data have been deliberately excluded from this data compilation to be able to use them as a  $\kappa_{OA}(M_{ac})$  model validation. In Fig. 10, where  $\kappa_{OA}$  is shown for  $M_{ac}$  ranging from 1.0 to 11, laboratory-scale jets are represented as circles, numerical simulations as diamonds, and rocket data are given as squares.

From these combined data in Fig. 10, representing an extremely wide range of jet conditions, a relationship between  $\kappa_{OA}$  and  $M_{ac}$  was sought. Although Ref. [16] used a log-based regression, the linear decrease roughly formed by the data when plotted on a log-log axis suggested a power-law regression with the form of

$$\kappa_{OA} = AM_{ac}^B \quad (17)$$

Solving for the coefficients  $A$  and  $B$  in Eq. (17) using a nonlinear least-squares regression resulted in  $A = 0.98 \pm 0.05$  and  $B = -0.48 \pm 0.06$  for the 95% confidence interval and an  $R^2$  value of 0.87. The fit and confidence bounds are the black and gray lines, respectively, in Fig. 10. Given that  $A \approx 1$  and  $B \approx -0.5$ , this regression can be written as

$$\kappa_{OA} \approx \frac{1}{\sqrt{M_{ac}}} \quad (18)$$

The result in Eq. (18) is startling in that  $\kappa_{OA}$  is no longer an ad hoc empirical parameter but rather depends only on the fully expanded jet velocity and the near-constant ambient sound speed. Substituting Eq. (18) into Eq. (15) reveals a new data-driven convective Mach number for supersonic jets ranging from laboratory conditions through rockets. The resulting Mach number is written as

$$M_\kappa \approx \sqrt{M_{ac}} \quad (19)$$

Again, Eq. (19) indicates that the convective Mach number for a convectively supersonic jet can be written in terms of  $u_j$  and  $c_a$  without the need to rely on an empirical constant,  $\kappa_{OA}$ . Assuming that a calculation of  $\theta_{max}$  within a few degrees is sufficiently accurate, this expression for supersonic jet convective Mach number represents a notable contribution of this paper. To determine the expected MWR angle accuracy and uncertainty, the  $M_\kappa$  obtained from the power-law fit has been converted to maximum angle  $\theta_{M_\kappa}$  and plotted in Fig. 11. The curve demonstrates that the 95% confidence angle span is approximately  $\pm 5^\circ$ , comparable to the angular measurement resolution for most experiments. As an important culminating example that demonstrates the utility of Eq. (19), the  $\theta_{max}$  from the T-7A measurement (see Table 1) are plotted against the associated  $M_{ac}$  for all four T-7A engine conditions. There is excellent agreement between the observed  $\theta_{max}$  and theory, with a maximum error of  $2.1^\circ$ , which is appreciably better than the measurement array resolution. Although it is impossible to state that Eq. (19) for convective Mach number is applicable to all supersonic jets, the database used to create the model spans a wide variety of physical and simulated jets and therefore represents a relatively robust database. Furthermore, its evaluation against the T-7A engine conditions ranging from intermediate thrust (38%) through AB represents a critical, successful benchmark case.

The convective Mach number definition in Eq. (19) is an empirical data-driven model, but it can be grounded in physics and directly connected to the  $M_{ac}$ -based expression for Oertel's  $M'_c$  in Eq. (10).

<sup>‡</sup>The results in Langenais et al. [35] were computed using a  $41.6 D_j$  virtual arc centered at the nozzle exit. The OASPL data have been transformed by shifting the arc center to  $14 D_j$  and accounting for spherical spreading about the shifted origin. This changes their reported peak radiation angle from  $40$  to  $60.3^\circ$ , consistent with results elsewhere in their paper.

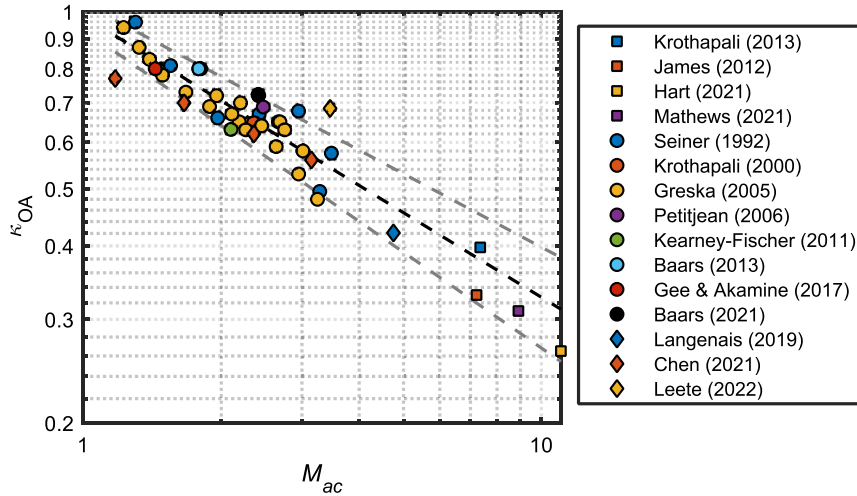


Fig. 10 The  $\kappa_{OA}$  as a function of  $M_{ac}$ . The black dashed line represents the power law fit with the 95% confidence interval bounds in gray.

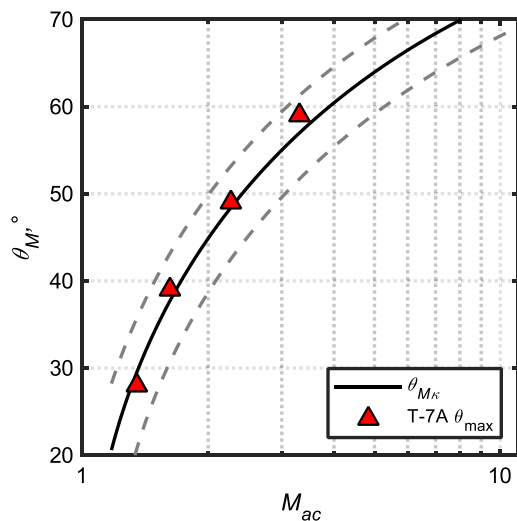


Fig. 11 Peak radiation angles from the regression in Fig. 10, along with the observed T-7A  $\theta_{max}$  for four engine conditions.

The first-order Taylor expansion for Eq. (19) about  $M_{ac} = 1$  may be written as

$$\sqrt{M_{ac}} \approx 1 + \frac{1}{2}(M_{ac} - 1) = \frac{M_{ac} + 1}{2} \quad (20)$$

In the limit as  $c_j/c_a \rightarrow 1$  (isothermal jets), Eq. (10) is identical to Eq. (20). Thus, the model for convective Mach number in Eq. (19) is a special case approximation for a more exact expression. But, whereas Eq. (10) requires knowledge of  $U_j$ ,  $c_j$ , and  $c_a$ , Eq. (19) only requires knowledge of one jet parameter,  $U_j$ . Even in cases where only exit conditions are known, such as for rockets where sea-level specific impulse is provided, this simpler expression is likely accurate within a couple of degrees.

What, then, is the error associated with making an isothermal jet approximation in using  $M_k \approx \sqrt{M_{ac}}$ ? The angle difference associated with Eqs. (10) and (19),  $\Delta\theta_M = |\theta_{M_c} - \theta_{M'_c}|$ , has been calculated for a wide range of  $M_{ac}$  and  $c_j/c_a$  and a contour map created in Fig. 12. The T-7A data points are shown as a reference, with a maximum error between the two Mach number models of  $\sim 2.5^\circ$  for AB. Because of the upward slope of the zero-error null with  $M_{ac}$ , it turns out that for most practical jets where temperature and velocity increase jointly, the error associated with neglecting sound speed differences in using Eq. (19) remains low—within  $2^\circ$ . To demonstrate this agreement, the Seiner et al. jet [23] and rocket data from Fig. 8 are

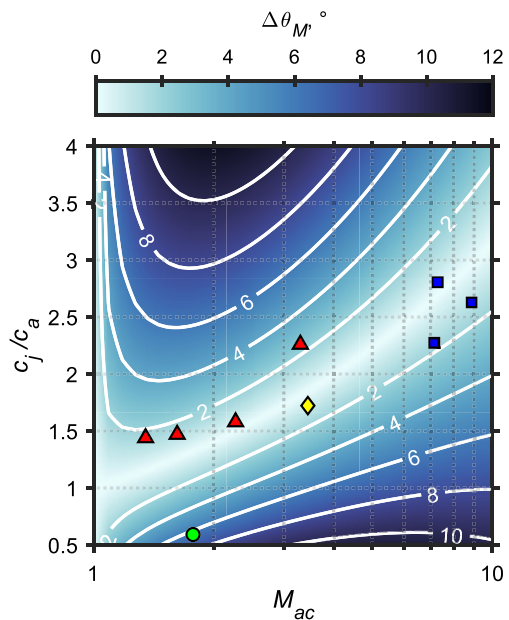


Fig. 12 Difference in  $\theta_M$  using the  $M'_c$  definition in Eq. (10) and the  $\sqrt{M_{ac}}$  approximation in Eq. (19), along with T-7A, Seiner, Baars, and rocket data from Fig. 8.

included in Fig. 12. The Baars et al. [26,27] Mach 3.0, unheated jet is also included as a green circle in Fig. 12. Even for this relatively extreme case, which deviates from the isothermal approximation,  $\Delta\theta_M \approx 6^\circ$ . However, it is worth noting that the difference between  $\theta_{max}$  and  $\theta_{M_c}$  for the Baars et al.'s jet is actually only  $4^\circ$ , as the measured peak directivity angle falls between  $\theta_{M'_c}$  and  $\theta_{M_c}$ . Overall, the analysis in Fig. 12 indicates that  $\theta_{max}$  is mostly determined by jet velocity and that temperature represents a relatively small correction, especially for heated jets.

## V. Conclusions

Using far-field T-7A noise data at different F404 engine conditions from 38% thrust through AB, this paper has reviewed and explored different convective Mach number definitions for supersonic jets. Based on Oertel's [17,18] three families of instability waves, only the K-H instability waves affect the T-7A's peak radiation angle. Supersonic instability waves, which travel slower than the K-H waves, are not present below AB for the T-7A, which explains why Greska's "Oertel convective Mach number" [29]—the arithmetic mean of the K-H and SI convective Mach numbers—does a poor job of predicting

radiation angle for jet conditions less than those of rockets. And, while Greska's convective amplification-based modification to the Oertel convective Mach number performed better in predicting the T-7A maximum directivity angle for multiple engine conditions, it performed no better than the K-H convective Mach number. There is evidence for Mach waves that travel faster than the K-H waves; it is possible that these are caused by velocity fluctuations in the shock cells, where the local jet velocity can exceed the fully expanded jet velocity.

Regarding the empirically derived ratio of convective-to-fully expanded velocities,  $\kappa = U_c/U_j$ , this analysis has shown that  $\kappa_{OA}$  decreases as the F404 engine power increases until reaching  $\kappa_{OA} \approx 0.6$  for AB. This value, similar to laboratory-scale studies of highly heated supersonic jets, falls between  $\kappa$  seen for unheated supersonic jets ( $\sim 0.8$ ) and rockets ( $\sim 0.3$ ). Curiously, these values approximately bound the frequency-dependent behavior of  $\kappa(f)$  for AB—reaching nearly 0.8 at high frequencies and 0.3 at low frequencies, with a rapid transition occurring at frequencies that are primarily generated between the potential and supersonic core tips. A similar transition was seen for  $\kappa(f)$  at military power, which agreed fairly well with a laboratory-scale analysis [49].

To explore how  $\kappa_{OA}$  changes with jet conditions from typical laboratory-scale conditions through rockets,  $\kappa$  values from several different studies were compiled and plotted as a function of jet acoustic Mach number  $M_{ac}$ , resulting in a new, data-driven definition of convective Mach number, which is simply  $\sqrt{M_{ac}}$ . The agreement with four convectively supersonic T-7A engine conditions, which were not used in the data fitting, is startlingly good, better than the approximately  $\pm 5^\circ$  95% confidence interval yielded by the fit. However, it turns out that the data-derived  $\sqrt{M_{ac}}$  is not entirely empirical. A comparison between a first-order Taylor series approximation for  $\sqrt{M_{ac}}$  and Oertel's expression for the K-H Mach waves shows that they are identical for an isothermal jet. This result helps establish the importance of jet velocity, relative to temperature, in determining maximum directivity angle from military-type jets and rockets.

### Acknowledgments

We gratefully acknowledge M. A. Christian for his preliminary work on this topic and thank Daniel Edgington-Mitchell of Monash University for helpful discussions regarding subsonic instability waves. Funding was provided by the Office of Naval Research under Grant No. N00014-21-1-2069 with project monitor Steven Martens, Code 351 Jet Noise Reduction. Measurements were funded through the Advanced Pilot Training System Program Office and the Air Force Research Laboratory. This research was supported in part by the appointment of L. T. M. to the Department of Defense (DOD) Research Participation Program administered by the Oak Ridge Institute for Science and Education (ORISE) through an interagency agreement between the U.S. Department of Energy (DOE) and the DOD. ORISE is managed by Oak Ridge Associated Universities (ORAU) under DOE contract number DE-SC0014664. All opinions expressed in this paper are the authors' and do not necessarily reflect the policies and views of DOD, DOE, or ORAU/ORISE. Distribution Statement A: Approved for public release; distribution unlimited.

### References

- [1] Wall, A. T., Gee, K. L., Morris, P. J., Colonius, T., and Lowe, K. T., "Introduction to the Special Issue on Supersonic Jet Noise," *Journal of the Acoustical Society of America*, Vol. 151, No. 2, Feb. 2022, pp. 806–816. <https://doi.org/10.1121/10.0009321>
- [2] Westley, R., and Lilley, G. M., "An Investigation of the Noise Field from a Small Jet and Methods for Its Reduction," College of Aeronautics, Cranfield Univ. Rept. 53, Cranfield, England, U.K., 1952.
- [3] Chobotov, V., and Powell, A., "On the Prediction of Acoustic Environments from Rockets," Rama-Wooldridge Corp. Rept. E.M.-7-7, 1957.
- [4] Cole, J. N., Von Gierke, H. E., Kyrzias, D. T., Eldred, K. M., and Humphrey, A. J., "Noise Radiation from Fourteen Types of Rockets in the 1,000 to 130,000 Pounds Thrust Range," Wright Air Development Center TR 57-354, AD 130794, 1957.
- [5] Laufer, J., "Aerodynamic Noise in Supersonic Wind Tunnels," *Journal of the Aerospace Sciences*, Vol. 28, No. 9, 1961, pp. 685–692. <https://doi.org/10.2514/8.9150>
- [6] Phillips, O. M., "On the Generation of Sound by Supersonic Turbulent Shear Layers," *Journal of Fluid Mechanics*, Vol. 9, March 1960, pp. 1–28. <https://doi.org/10.1017/S0022112060000888>
- [7] Ffowcs Williams, J. E., "The Noise from Turbulence Convected at High Speed," *Philosophical Transactions A*, Vol. 1061, No. 255, 1963, pp. 641–657. <https://doi.org/10.1098/rsta.1963.0010>
- [8] Tam, C. K. W., "Supersonic Jet Noise," *Annual Review of Fluid Mechanics*, Vol. 27, Jan. 1995, pp. 17–43. <https://doi.org/10.1146/annurev.fl.27.010195.000313>
- [9] Bailly, C., and Fujii, K., "High-Speed Jet Noise," *Mechanical Engineering Reviews*, Vol. 3, No. 1, 2016, pp. 1–13. <https://doi.org/10.1299/mer.15-00496>
- [10] Lubert, C. P., Gee, K. L., and Tsutsumi, S., "Supersonic Jet Noise from Launch Vehicle: 50 Years Since NASA SP-8072," *Journal of the Acoustical Society of America*, Vol. 151, No. 2, 2022, pp. 752–791. <https://doi.org/10.1121/10.0009160>
- [11] Liu, J., Corrigan, A., Kailasanath, K., and Taylor, B., "Impact of the Specific Heat Ratio on the Noise Generation in a High-Temperature Supersonic Jet," *54th AIAA Aerospace Sciences Meeting*, AIAA Paper 2016-2125, Jan. 2016. <https://doi.org/10.2514/6.2016-2125>
- [12] Kearney-Fischer, M., Kim, J. H., and Samimy, M., "A Study of Mach Wave Radiation Using Active Control," *Journal of Fluid Mechanics*, Vol. 681, June 2011, pp. 261–292. <https://doi.org/10.1017/jfm.2011.196>
- [13] Krothapalli, A., Arakeri, V., and Greska, B., "Mach Wave Radiation: A Review and an Extension," *41st Aerospace Sciences Meeting and Exhibit*, AIAA Paper 2003-1200, Jan. 2003. <https://doi.org/10.2514/6.2003-1200>
- [14] Viswanathan, K., "Aeroacoustics of Hot Jets," *Journal of Fluid Mechanics*, Vol. 516, Sept. 2004, pp. 39–82. <https://doi.org/10.1017/S0022112004000151>
- [15] Tam, C. K. W., "Mach Wave Radiation from High-Speed Jets," *AIAA Journal*, Vol. 47, No. 10, 2009, pp. 2440–2448. <https://doi.org/10.2514/1.42644>
- [16] Christian, M. A., and Gee, K. L., "Connecting the Convective Mach Number to Full-Scale Supersonic Jet Noise Directivity," *AIAA Aviation Forum*, AIAA Paper 2023-3351, June 2023. <https://doi.org/10.2514/6.2023-3351>
- [17] Oertel, H., "Machwave Radiation of Hot Supersonic Jets Investigated by Means of the Shock Tube and New Optical Techniques," *12th International Symposium on Shock Tubes and Waves*, July 1980, pp. 266–275.
- [18] Oertel, H., "Measured Velocity Fluctuations Inside the Mixing Layer of a Supersonic Jet," *Recent Contributions to Fluid Mechanics*, Vol. 1, 1982, pp. 170–179.
- [19] Tam, C. K. W., and Hu, F. Q., "On the Three Families of Instability Waves of High-Speed Jets," *Journal of Fluid Mechanics*, Vol. 201, April 1989, pp. 447–483. <https://doi.org/10.1017/S002211208900100X>
- [20] Papamoschou, D., and Roshko, A., "The Compressible Turbulent Shear Layer: An Experimental Study," *Journal of Fluid Mechanics*, Vol. 197, April 1988, pp. 453–477. <https://doi.org/10.1017/S0022112088003325>
- [21] Towne, A., Cavalieri, A. V., Jordan, P., Colonius, T., Schmidt, O., Jaunet, V., and Brès, G. A., "Acoustic Resonance in the Potential Core of Subsonic Jets," *Journal of Fluid Mechanics*, Vol. 825, July 2017, pp. 1113–1152. <https://doi.org/10.1017/jfm.2017.346>
- [22] Nogueira, P. A. S., Cavalieri, A. V. G., Martini, E., Towne, A., Jordan, P., and Edgington-Mitchell, D., "Guided Jet Waves," *Journal of Fluid Mechanics*, Vol. 999, Nov. 2024. <https://doi.org/10.1017/jfm.2024.797>
- [23] Seiner, J. M., Ponton, M. K., Jansen, B. J., and Lagen, N. T., "The Effects of Temperature on Supersonic Jet Noise Emission," *14th Aachen*, Vol. 1 (A93-19126 05-71), AIAA Paper 92-02-046, May 1992, pp. 295–307.
- [24] Oertel Sen, H., Seiler, F., Srulijes, J., and Hruschka, R., "Mach Waves Produced in the Supersonic Jet Mixing Layer by Shock/Vortex Interaction," *Shock Waves*, Vol. 26, Feb. 2016, pp. 231–240. <https://doi.org/10.1007/s00193-015-0612-1>
- [25] Rohatgi, A., "WebPlotDigitizer Version 2.6," Sept. 2022, <https://automeris.io/WebPlotDigitizer>.
- [26] Baars, W. J., "Acoustics from High-Speed Jets with Crackle," Ph.D. Dissertation, Univ. of Texas at Austin, Austin, TX, 2013.

- [27] Baars, W. J., Tinney, C. E., Wochner, M. S., and Hamilton, M. F., "On cumulative Nonlinear Acoustic Waveform Distortions from High-Speed Jets," *Journal of Fluid Mechanics*, Vol. 749, May 2014, pp. 331–366. <https://doi.org/10.1017/jfm.2014.228>
- [28] Pineau, P., and Bogey, C., "Numerical Investigation of Wave Steepening and Shock Coalescence near a Cold Mach 3 Jet," *Journal of the Acoustical Society of America*, Vol. 149, No. 1, 2021, pp. 357–370. <https://doi.org/10.1121/10.0003343>
- [29] Greska, B. J., "Supersonic Jet Noise and Its Reduction Using Microjet Injection," Ph.D. Dissertation, Florida State Univ., Tallahassee, FL, 2005.
- [30] Greska, B., Krothapalli, A., Horne, W. C., and Burnside, N., "A Near-Field Study of High Temperature Supersonic Jets," *14th AIAA/CEAS Aeroacoustics Conference*, AIAA Paper 2008-3026, May 2008. <https://doi.org/10.2514/6.2008-3026>
- [31] Krothapalli, A., Venkatakrishnan, L., Lourenco, L., Greska, B., and Elavarasan, R., "Turbulence and Noise Suppression of a High-Speed Jet by Water Injection," *Journal of Fluid Mechanics*, Vol. 491, 2003, pp. 131–159. <https://doi.org/10.1017/S0022112003005226>
- [32] Liu, J., Kailasanath, K., Munday, D., Heeb, N., and Gutmark, E., "Large-Eddy Simulations of a Supersonic Heated Jet," *17th AIAA/CEAS Aeroacoustics Conference*, AIAA Paper 2011-2884, June 2011. <https://doi.org/10.2514/6.2011-2884>
- [33] Papamoschou, D., and Roshko, A., "The Compressible Turbulent Shear Layer: An Experimental Study," *Journal of Fluid Mechanics*, Vol. 197, April 1988, pp. 453–477. <https://doi.org/10.1017/S0022112088003325>
- [34] Strykowski, P. J., Krothapalli, A., and Jendoubi, S., "The Effect of Counterflow on the Development of Compressible Shear Layers," *Journal of Fluid Mechanics*, Vol. 308, April 1996, pp. 63–96. <https://doi.org/10.1017/S0022112096001395>
- [35] Langenais, A., François, V., Troyes, J., and Bailly, C., "Accurate Simulation of the Noise Generated by a Hot Supersonic Jet Including Turbulence Tripping and Nonlinear Acoustic Propagation," *Physics of Fluids*, Vol. 31, Jan. 2019, Paper 016105. <https://doi.org/10.1063/1.5050905>
- [36] James, M. M., Salton, A. R., Gee, K. L., Neilsen, T. B., McNerny, S. A., and Kenny, R. J., "Modification of Directivity Curves for a Rocket Noise Model," *Proceedings of Meetings on Acoustics*, Vol. 18, March 2012. <https://doi.org/10.1121/1.4870986>
- [37] Hart, G. W., Mathews, L. T., Anderson, M. C., Durrant, T., Bassett, M. S., Olausson, S. A., Houston, G., and Gee, K. L., "Methods and Results of Acoustical Measurements Made of a Delta IV Heavy Launch," *Proceedings of Meetings on Acoustics*, Vol. 45, July 2021. <https://doi.org/10.1121/2.0001580>
- [38] Bassett, M. S., Gee, K. L., Hart, G. W., Mathews, L. T., Rasband, R. D., and Novakovich, D. J., "Peak Directivity Analysis of Far-Field Acoustical Measurements During Three GEM 63 Static Firings," *Proceedings of Meetings on Acoustics*, Vol. 39, Sept. 2019. <https://doi.org/10.1121/2.0001467>
- [39] Pineau, P., and Bogey, C., "Temperature Effects on Convection Speed and Steepened Waves of Temporally Developing Supersonic Jets," *AIAA Journal*, Vol. 58, No. 3, Dec. 2020, pp. 1227–1239. <https://doi.org/10.2514/1.J058589>
- [40] Liu, J., Corrigan, A., Kailasanath, K., and Gutmark, E., "Effects of Temperature on Noise Generation in Supersonic Jets," *22nd AIAA/CEAS Aeroacoustics Conference*, AIAA Paper 2016-2937, May–June 2016. <https://doi.org/10.2514/6.2016-2937>
- [41] Ecker, T., Lowe, K. T., and Ng, W. F., "Eddy Convection in Developing Heated Supersonic Jets," *AIAA Journal*, Vol. 53, No. 11, 2015, pp. 3305–3315. <https://doi.org/10.2514/1.J053946>
- [42] Chen, S., Gojon, R., and Mihaescu, M., "Flow and Aeroacoustic Attributes of Highly-Heated Transitional Rectangular Supersonic Jets," *Aerospace Science and Technology*, Vol. 114, July 2021, Paper 106747. <https://doi.org/10.1016/j.ast.2021.106747>
- [43] Murray, N. E., and Lyons, G. W., "On the Convection Velocity of Source Events Related to Supersonic Jet Crackle," *Journal of Fluid Mechanics*, Vol. 793, March 2016, pp. 477–503. <https://doi.org/10.1017/jfm.2016.127>
- [44] Tam, C. K. W., and Parrish, S. A., "Noise of High-Performance Aircraft at Afterburner," *Journal of Sound and Vibration*, Vol. 352, Sept. 2015, pp. 103–128. <https://doi.org/10.1016/j.jsv.2015.04.010>
- [45] Papamoschou, D., Morris, P. J., and McLaughlin, D. K., "Beamformed Flow-Acoustic Correlations in a Supersonic Jet," *AIAA Journal*, Vol. 48, No. 10, 2010, pp. 2445–2453. <https://doi.org/10.2514/1.J050325>
- [46] Mathews, L. T., Gee, K. L., and Hart, G. W., "Characterization of Falcon 9 Launch Vehicle Noise from Far-Field Measurements," *Journal of the Acoustical Society of America*, Vol. 150, July 2021, pp. 620–633. <https://doi.org/10.1121/10.0005658>
- [47] Morris, P. J., "A Note on Noise Generation by Large Scale Turbulent Structures in Subsonic and Supersonic Jets," *International Journal of Aeroacoustics*, Vol. 8, No. 4, 2009, pp. 301–315. <https://doi.org/10.1260/147547209787548921>
- [48] Neilsen, T. B., Vaughn, A. B., Gee, K. L., Akamine, M., Okamoto, K., Teramoto, S., and Tsutsumi, S., "Data-Educed Broadband Equivalent Acoustic Source Model for Supersonic Jet Noise," *Journal of the Acoustical Society of America*, Vol. 146, No. 5, 2019, pp. 3409–3424. <https://doi.org/10.1121/1.5132947>
- [49] Baars, W. J., Murray, N. E., and Tinney, C. E., "A Proper Framework for Studying Noise from Jets with Non-Compact Sources," *Journal of Fluid Mechanics*, Vol. 929, Oct. 2021, p. A23. <https://doi.org/10.1017/jfm.2021.837>
- [50] Greska, B. J., Krothapalli, A., Seiner, J. M., Jansen, B., and Ukeiley, L., "The Effects of Microjet Injection on an F404 Jet Engine," *11th AIAA/CEAS Aeroacoustics Conference (26th AIAA Aeroacoustics Conference)*, AIAA Paper 2005-3047, May 2005. <https://doi.org/10.2514/6.2005-3047>
- [51] Seiner, J. M., Ukeiley, L. S., and Jansen, B. J., "Aero-Performance Efficient Noise Reduction for the F404-400 Engine," *11th AIAA/CEAS Aeroacoustics Conference (26th AIAA Aeroacoustics Conference)*, AIAA Paper 2005-3048, May 2005. <https://doi.org/10.2514/6.2005-3048>
- [52] Greska, B., and Krothapalli, A., "On the Far-Field Propagation of High-Speed Jet Noise," *ASME 2008 Noise Control and Acoustics Division Conference*, NCAD Paper 2008-73071, July 2008. <https://doi.org/10.1115/NCAD2008-73071>
- [53] Podboy, G. G., Bridges, J. E., and Henderson, B. S., "Phased Array Noise Source Localization Measurements of an F404 Nozzle Plume at Both Full and Model Scale," *ASME Turbo Expo 2010: Power for Land, Sea, and Air*, Dec. 2010. <https://doi.org/10.1115/GT2010-22601>
- [54] Powers, R. W., Kuo, C. W., and McLaughlin, D. K., "Experimental Comparison of Supersonic Jets Exhausting from Military Style Nozzles with Interior Corrugations and Fluidic Inserts," *19th AIAA/CEAS Aeroacoustics Conference*, AIAA Paper 2013-2186, May 2013. <https://doi.org/10.2514/6.2013-2186>
- [55] Liu, J., Johnson, R. F., and Ramamurti, R., "Numerical Study of Supersonic Jet Noise Emanating from an F404 Nozzle at Model Scale," *AIAA SciTech 2019 Forum*, AIAA Paper 2019-0807, Jan. 2019. <https://doi.org/10.2514/6.2019-0807>
- [56] Brès, G. A., Towne, A., and Lele, S. K., "Investigating the Effects of Temperature Non-Uniformity on Supersonic Jet Noise with Large-Eddy Simulation," *25th AIAA/CEAS Aeroacoustics Conference*, AIAA Paper 2019-2730, May 2019. <https://doi.org/10.2514/6.2019-2730>
- [57] Liu, J., and Martens, S., "Noise Reduction by Lowering the Jet Mach Number at Fixed Thrust and Mass Flow," *AIAA Aviation 2023 Forum*, AIAA Paper 2023-4515, June 2023. <https://doi.org/10.2514/6.2023-4515>
- [58] Leete, K. M., Vaughn, A. B., Bassett, M. S., Rasband, R. D., Novakovich, D. J., Gee, K. L., Campbell, S. C., Mobley, F. S., and Wall, A. T., "Jet Noise Measurements of an Installed GE F404 Engine," *AIAA SciTech 2021 Forum*, AIAA Paper 2021-1638, Jan. 2021. <https://doi.org/10.2514/6.2021-1638>
- [59] Wall, A. T., Gee, K. L., James, M. M., Bradley, K. A., McNerny, S. A., and Neilsen, T. B., "Near-Field Noise Measurements of a High-Performance Military Jet Aircraft," *Noise Control Engineering Journal*, Vol. 60, No. 4, 2012, pp. 421–434. <https://doi.org/10.3397/1.3701021>
- [60] "Numerical Propulsion System Simulation (NPSS)," Southwest Research Institute, <https://www.swri.org/consortia/numerical-propulsion-system-simulation-npss>.
- [61] Christian, M. A., Gee, K. L., Streeter, J. B., Wall, A. T., and Campbell, S. C., "Sound Power and Acoustic Efficiency of an Installed GE F404 Jet Engine," *JASA Express Letters*, Vol. 3, No. 7, July 2023, Paper 073601. <https://doi.org/10.1121/10.0019866>
- [62] Streeter, J. B., Christian, M. A., Gee, K. L., Wall, A. T., and Campbell, S. C., "Assessing Impact of Near-Ground Meteorology on Spectral Variability in Static Jet Aircraft Noise Measurements," *Proceedings of Meetings on Acoustics*, Vol. 50, 2022, Paper 040010.
- [63] "Methods for the Measurement of Noise Emissions from High Performance Military Jet Aircraft," ANSI ASA S12.75-2012 (R2020), Acoustical Soc. of America, Melville, NY, 2020, <https://webstore.ansi.org/standards/asa/asiasas12752012?srsltid=AfmBOorvPTgmPUSel8x-gg2o0-JkInZRJbXbON4RyXpYJj397N79R58>.

- [64] Christian, M. A., Gee, K. L., Streeter, J. B., Wall, A. T., and Campbell, S. C., "Implementing a Heuristic Method to Correct Ground Reflection Effects Observed in Full-Scale Tactical Aircraft Noise Measurements," *Proceedings of Meetings on Acoustics*, Vol. 50, No. 1, Dec. 2022, Paper 040005. <https://doi.org/10.1121/2.0001750>
- [65] Gee, K. L., Neilsen, T. B., and James, M. M., "Including Source Correlation and Atmospheric Turbulence in a Ground Reflection Model for Rocket Noise," *Proceedings of Meetings on Acoustics*, Vol. 22, Nov. 2014, Paper 040001. <https://doi.org/10.1121/2.0000002>
- [66] James, M. M., Salton, A. R., Downing, J. M., Gee, K. L., Neilsen, T. B., Reichman, B. O., McKinley, R., Wall, A. T., and Gallagher, H., "Acoustic Emissions from F-35 Aircraft During Ground Run-Up," *2st AIAA/CEAS Aeroacoustics Conference*, AIAA Paper 2015-2375, June 2015. <https://doi.org/10.2514/6.2015-2375>
- [67] Vaughn, A. B., Gee, K. L., Swift, S. H., Leete, K. M., Wall, A. T., Downing, J. M., and James, M. M., "Source Localization of Crackle-Related Events in Military Aircraft Jet Noise," *AIAA Journal*, Vol. 59, No. 6, 2021, pp. 2251–2261. <https://doi.org/10.2514/1.J059823>
- [68] Hart, G. W., Gee, K. L., and Cook, M. R., "Corrected Frequency-Dependent Directivity Indices for Large Solid Rocket Motors," *Proceedings of Meetings on Acoustics*, Vol. 51, No. 1, May 2023, Paper 040007. <https://doi.org/10.1121/2.0001810>
- [69] Mathews, L. T., and Gee, K. L., "Acoustical Holography and Coherence-Based Noise Source Characterization of an Installed F404 Engine," *AIAA Journal*, Vol. 62, No. 6, 2024, pp. 2186–2199. <https://doi.org/10.2514/1.J063543>
- [70] Mathews, L. T., Gee, K. L., Leete, K. M., and Wall, A. T., "Acoustic Source Characterization of an Installed GE F404 Engine Using Near-Field Acoustical Holography," *28th AIAA/CEAS Aeroacoustics 2022 Conference*, AIAA Paper 2022-3028, 2022. <https://doi.org/10.2514/6.2022-3028>
- [71] Lighthill, M. J., "On Sound Generated Aerodynamically I: General Theory," *Proceedings of the Royal Society of London. Series A. Mathematical and Physical Sciences*, Vol. 211, No. 1107, 1952, pp. 564–587. <https://doi.org/10.1098/rspa.1952.0060>
- [72] Leete, K. M., Gee, K. L., Liu, J., and Wall, A. T., "Near-Field Acoustical Holography and Acoustic Power Analysis of a Simulated, Highly Heated Supersonic Jet," *Journal of the Acoustical Society of America*, Vol. 151, No. 3, 2022, pp. 1989–2001. <https://doi.org/10.1121/10.0009827>
- [73] Olaveson, T., Ward, J., Johnson, J., Gee, K. L., and Wall, A. T., "Analysis of Spatiotemporal Lobes in Installed F404 Engine Noise Radiation," *28th AIAA/CEAS Aeroacoustics 2022 Conference*, AIAA Paper 2022-3087, 2022. <https://doi.org/10.2514/6.2022-3087>
- [74] Olaveson, T. W., and Gee, K. L., "Wavelet-Based Characterization of Spatiotemporal Structures in F404 Engine Jet Noise," *AIAA Journal*, Vol. 62, No. 11, Nov. 2024.
- [75] Leete, K. M., Wall, A. T., Gee, K. L., Neilsen, T. B., James, M. M., and Downing, J. M., "Acoustical Holography-Based Analysis of Spatiotemporal Lobes in High-Performance Aircraft Jet Noise," *AIAA Journal*, Vol. 59, No. 10, 2021, pp. 4166–4178. <https://doi.org/10.2514/1.J059400>
- [76] Wall, A. T., Gee, K. L., Neilsen, T. B., McKinley, R. L., and James, M. M., "Military Jet Noise Source Imaging Using Multisource Statistically Optimized Near-Field Acoustical Holography," *Journal of the Acoustical Society of America*, Vol. 139, April 2016, pp. 1938–1950. <https://doi.org/10.1121/1.4945719>
- [77] Swift, S. H., Gee, K. L., Neilsen, T. B., Wall, A. T., Downing, J. M., and James, M. M., "Spatiotemporal-Correlation Analysis of Jet Noise from a Round Nozzle High-Performance Aircraft," *AIAA Aviation Forum*, AIAA Paper 2018-3938, 2018. <https://doi.org/10.2514/6.2018-3938>
- [78] Leete, K. M., Gee, K. L., Liu, J., and Wall, A. T., "Coherence Analysis of the Noise from a Simulated Highly Heated Laboratory-Scale Jet," *AIAA Journal*, Vol. 58, No. 8, 2020, pp. 3426–3435. <https://doi.org/10.2514/1.J059112>
- [79] Gee, K. L., Akamine, M., Okamoto, K., Neilsen, T. B., Cook, M. R., Tsutsumi, S., Teramoto, S., and Okunuki, T., "Characterization of Supersonic Laboratory-Scale Jet Noise with Vector Acoustic Intensity," *23rd AIAA/CEAS Aeroacoustics Conference*, AIAA Paper 2017-3519, 2017. <https://doi.org/10.2514/6.2017-3519>
- [80] Petitjean, B. P., Viswanathan, K., and McLaughlin, D. K., "Acoustic Pressure Waveforms Measured in High Speed Jet Noise Experiencing Nonlinear Propagation," *International Journal of Aeroacoustics*, Vol. 5, No. 2, 2006, pp. 193–215. <https://doi.org/10.1260/147547206777629835>
- [81] Krothapalli, A., Venkatakrishnan, L., and Lourenco, L., "Crackle: A Dominant Component of Supersonic Jet Mixing Noise," *6th Aeroacoustics Conference and Exhibit*, AIAA Paper 2000-2024, 2000. <https://doi.org/10.2514/6.2000-2024>

M. M. Choudhari  
Associate Editor